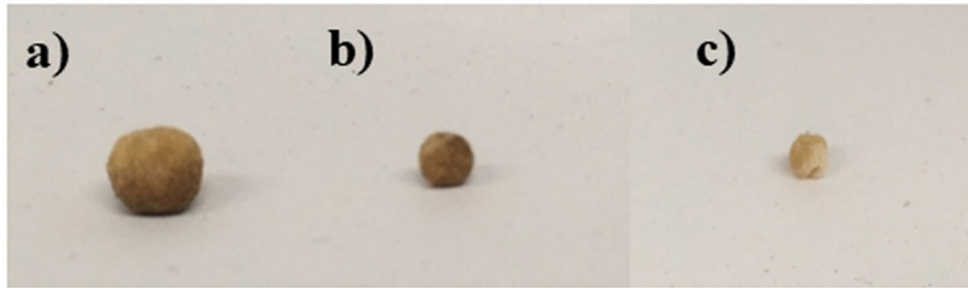


# Supporting Information

**A lottery draw machine-inspired movable air filter  
with high removal efficiency and low pressure drop  
at high flow rate**

*Nara Han,<sup>a</sup> Yo Seph Lee,<sup>a</sup> Byung Kwon Kaang,<sup>a</sup> Wooree Jang,<sup>b</sup> Hye Young Koo,<sup>b</sup> and Won  
San Choi<sup>\*,a</sup>*



**Fig. S1** Images of spherical MFS/NPs with various sizes of (a) 7 mm, (b) 3 mm, and (c) 1.5 mm.

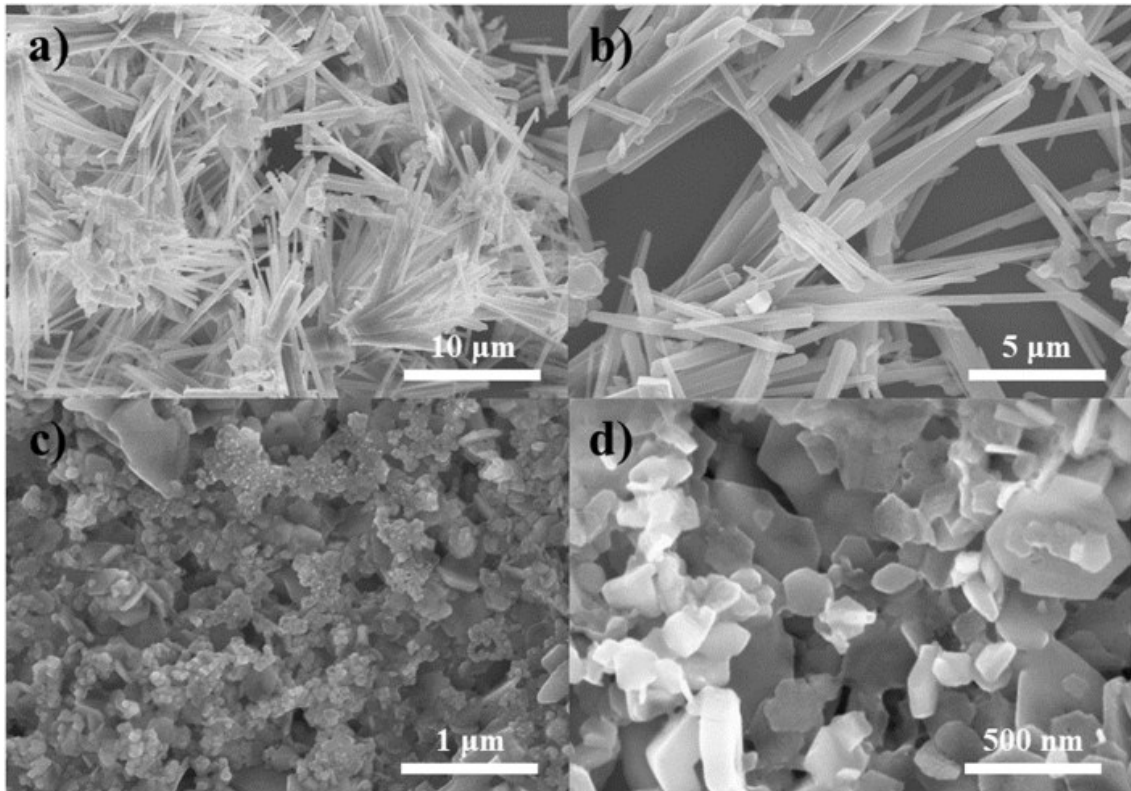


**Fig. S2** SEM images of (a, b) CaCO<sub>3</sub> precipitates and (c, d) Ag/Pt/Pd precipitates.



**Fig. S3** Images showing delivery of PM-laden polluted air from left source chamber to right detection chambers by air flow.

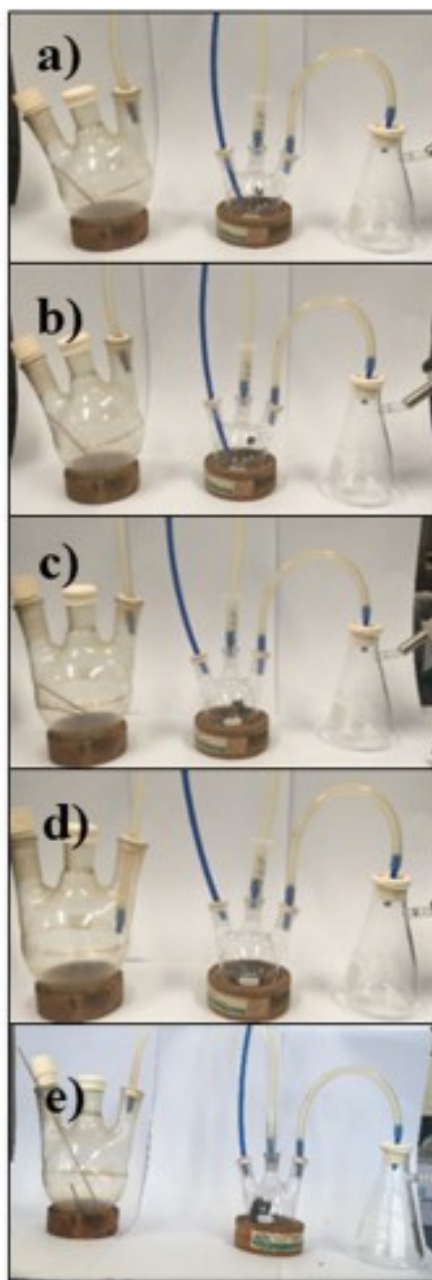


**Fig. S4** Images showing the air filtration system containing a different sized (volume) (a) cubic MFS-10, (b) cubic MFS-30, (c) cubic MFS-50, (d) cubic MFS-100, or (e) cubic MFS-120.

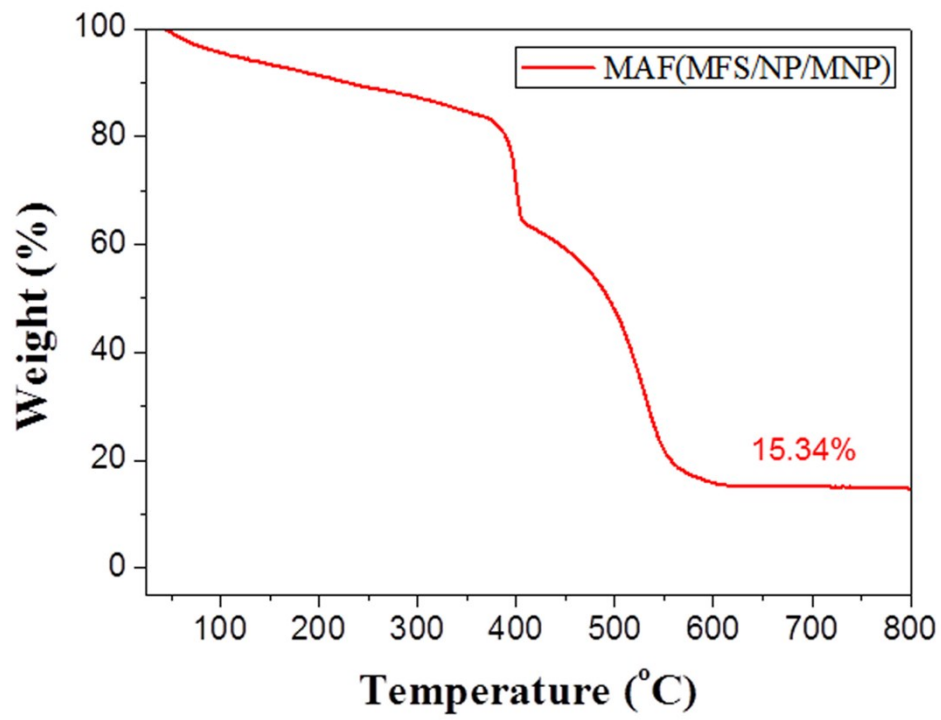


**Fig. S5** TGA data of MAF (MFS/NP/MNP) after movement or rotation of the MAFs for 1 h.

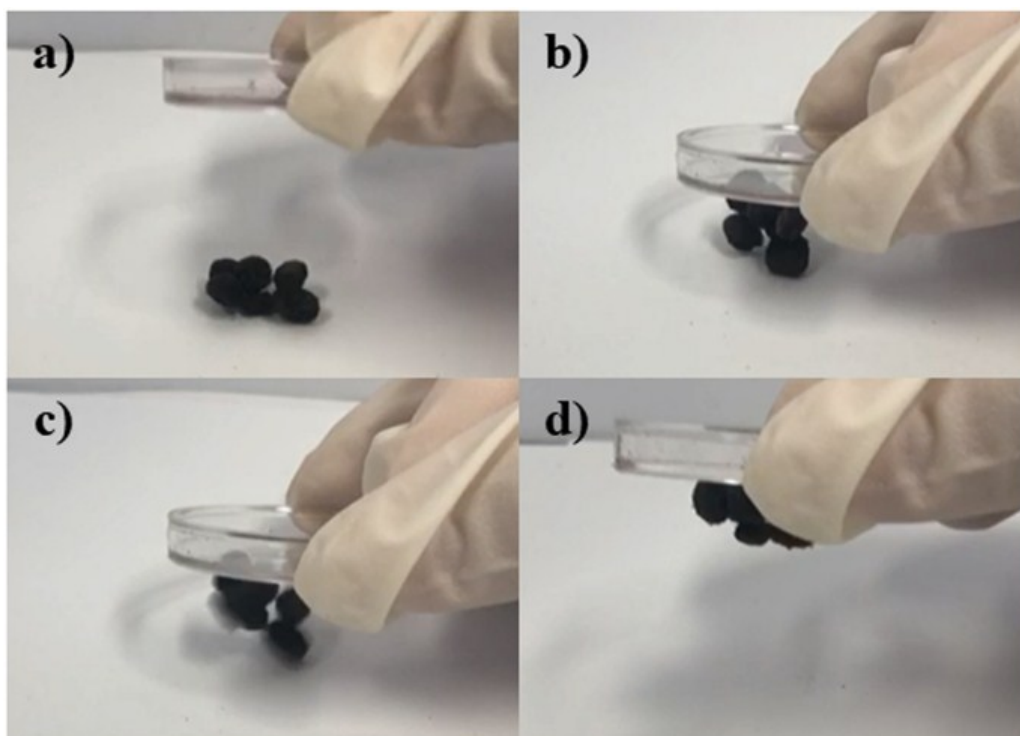


**Fig. S6** Images showing the electrostatic effects of MAFs when the surrounding object approached MAFs that immediately removed from the chamber. The MAFs were readily attracted to the surrounding object after rotation of MAFs within the chamber for 1 min because their strong electrostatic effects.

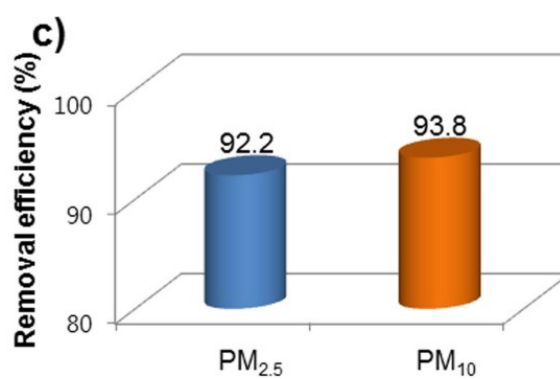
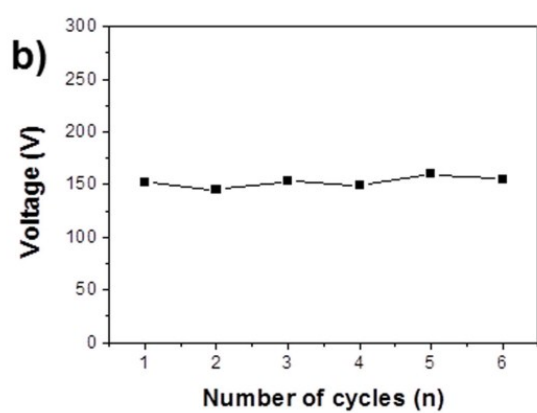


**Fig. S7** (a) A image showing the movable air filtration system based on the stainless steel chamber. (b) Surface potentials and (c) PM removal efficiencies of MAF-120 obtained in stainless steel chamber.



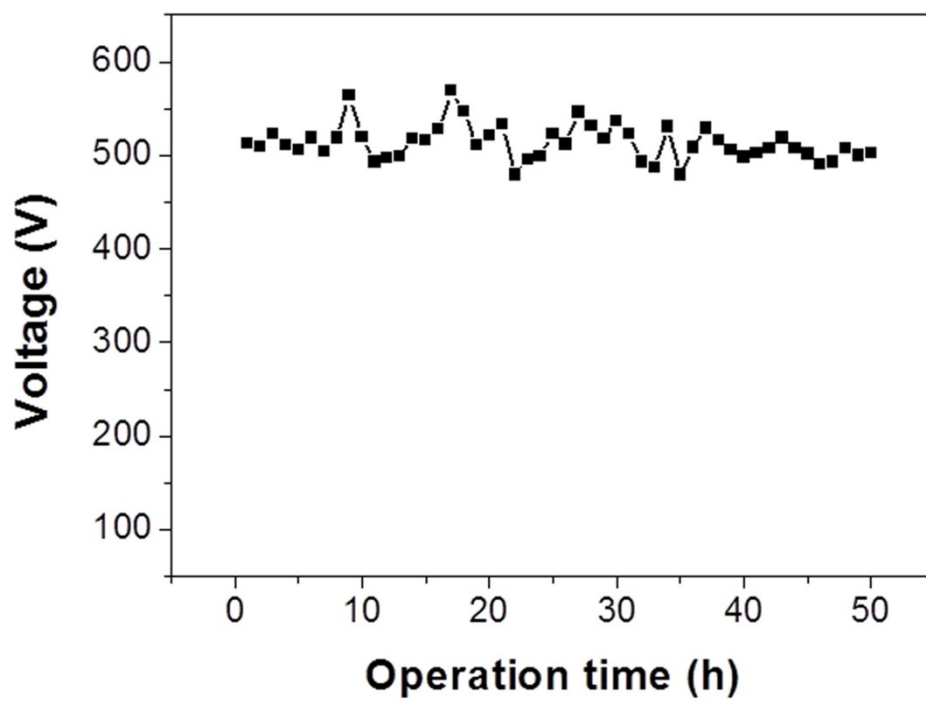


**Fig. S8** Surface potentials of MAF-120 measured during the long-term performance test.

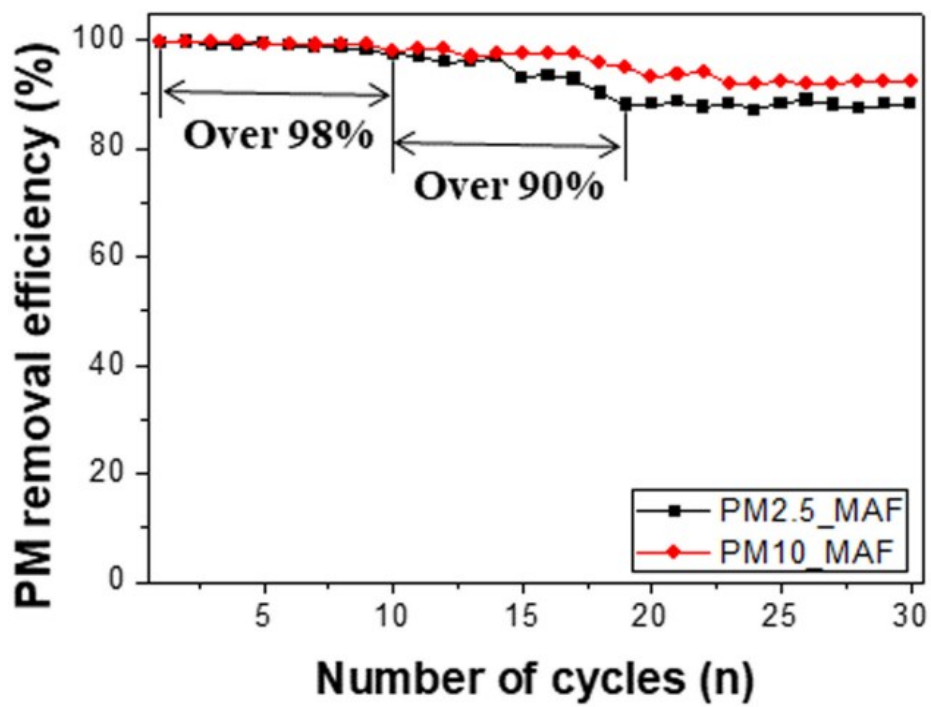


Fig. S9 PM<sub>2.5</sub> removal efficiency of MAF-120 in the absence of washing step.